Room-Temperature Giant Persistent Photoconductivity in $SrTiO_3/LaAlO_3$ Heterostructures

Antonello Tebano,[†,§] Emiliana Fabbri,[‡,§] Daniele Pergolesi,[‡,§] Giuseppe Balestrino,[†,*] and Enrico Traversa[‡,*]

[†]CNR-SPIN and Dipartimento di Informatica Sistemi e Produzione, University of Roma Tor Vergata, Rome, Italy, and [‡]International Research Center for Materials Nanoarchitectonics (MANA), National Institute for Materials Science (NIMS), Tsukuba, Japan. [§]These authors contributed equally to this work.

ABSTRACT

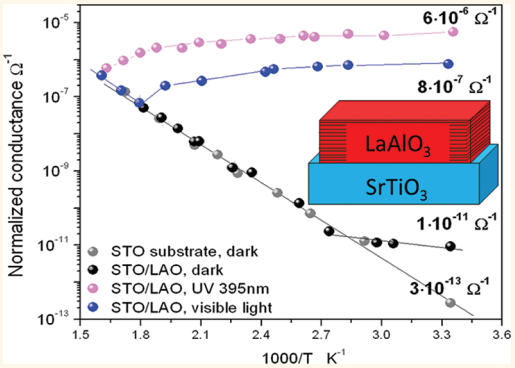

$SrTiO_3/LaAlO_3$ interfaces show an unprecedented photoconductivity effect that is persistent even at room temperature and giant as it gives rise to a conductivity increase of about 5 orders of magnitude at room temperature. The persistent photoconductivity effects play a paramount role in the still controversial intrinsic behavior of the $SrTiO_3/LaAlO_3$ interfaces, as even a limited exposure to visible light is able to strongly modify the electrical transport properties of the interface even above room temperature, while only an appropriate thermal treatment in a dark environment can completely suppress the persistent photoconductivity effect unveiling the intrinsic conduction mechanism of the interface. Moreover, our study demonstrates that the origin of the high conductivity, revealed at the STO/LAO interface at room temperature, is purely electronic.

KEYWORDS: $SrTiO_3/LaAlO_3$ interfaces · persistent photocurrent · electrochemical impedance spectroscopy

Persistent photocurrent (PPC) consists in a photoinduced increase in the electrical conductivity that persists after switching off the illumination, often with immeasurably long time constants.[1] Several semiconductor-based heterostructures, such as conducting GaAs on Cr-doped semi-insulating GaAs substrates[2] and AlGaAs/GaN,[3] exhibit PPC. In these systems the phenomenon is truly persistent only below room temperature, while at room temperature photocurrent decays with a characteristic time of thousands of seconds. PPC phenomena have been observed in other semiconducting systems, such as GaN nanowires[4] and, more recently, rough silicon nanomembranes.[5] In the latter case a giant photoinduced increase in conductivity, approximately 3 orders of magnitude larger than the dark conductivity, was measured. PPC effects have been measured in oxide systems too: photoinduced superconductivity, connected with the occurrence of PPC, has been demonstrated in underdoped $YBa_2Cu_3O_{7-x}$,[6] and an enhancement of photoconductivity was observed at the interface between $SrTiO_3$ and amorphous $CaHfO_3$, albeit only when fabricated by pulsed laser deposition.[7]

PPC in semiconducting heterostructures is ascribed to two main mechanisms: (a) the existence of macroscopic potential barriers due to junctions, surface barriers or doping inhomogeneities that spatially separate the photogenerated electron/hole pair, or the photoexcited carrier from the parent donor/acceptor defect,[2] and (b) the existence of potential barriers located at the atomic scale at centers with large lattice relaxation, where the empty defect level lies above the minimum of the conduction band and the occupied level lies within the band gap.[8]

A PPC effect based on the "a" mechanism, due to a possible charge-separation effect, can be envisaged also in the case of the interface between an epitaxial $LaAlO_3$ (LAO) film grown on a TiO_2-terminated (001) $SrTiO_3$ (STO) substrate. Epitaxial $LaAlO_3$ (LAO) films grown on a TiO_2-terminated (001) $SrTiO_3$ (STO) substrate have received great attention in the past decade. Both STO and LAO are band insulators, even though STO shows a small residual mixed ionic/electronic conductivity above room temperature. When the thickness of the LAO film exceeds four unit cells, a highly mobile, quasi-two-dimensional electron gas (q2DEG) is formed at the interface between the two perovskite-type oxides.[9,10]

* Address correspondence to balestrino@uniroma2.it, traversa.enrico@nims.go.jp.

Received for review October 17, 2011 and accepted January 19, 2012.

Published online January 19, 2012
10.1021/nn203991q

Such a positively charged interface layer is compensated by a negative electronic space charge region. This negative electronic space charge region is responsible for the q2DEG, which extends several nm below the interface and gives rise to an electrical dipole region with an associated potential barrier. Mainly three possible mechanisms at the origin of such a q2DEG at the interface have been proposed, but a full consensus has not been reached yet. The first mechanism is based on the polarity discontinuity at the interface between the nonpolar sequence of atomic planes in the substrate ($SrO^0/TiO_2{}^0$) and the polar sequence in the film ($LaO^{+1}/AlO_2{}^{-1}$).[11] Such a discontinuity is expected to give rise to an electrostatic potential in the LAO film that diverges with thickness. A divergence catastrophe at the $AlO_2/LaO/TiO_2$ interface is avoided by adding half an electron per formula unit to the TiO_2 interface layer. A second mechanism foresees the formation of a high density of oxygen vacancies in the STO substrate.[12,13] Namely, for LAO films grown on a STO substrate at a background oxygen pressure below 10^{-3}–10^{-4} mbar, a high concentration of oxygen vacancies is originated in the substrate bulk that gives rise to n-doping and to an increase of several orders of magnitude of its bulk electrical conductivity.[14] Recently, an oxygen transfer between the substrate and the as-grown thin film was observed for $SrTiO_3$ and $LaAlO_3$ thin films, deposited onto $SrTiO_3$ and $LaAlO_3$ substrates, indicating that the film is oxygen deficient and a chemical gradient favors oxygen supply *via* the substrate.[15] Cathode-luminescence measurements[16,17] on LAO/STO heterostructures have shown the presence of a strong blue light signal peaked at 460 nm. This signal was ascribed to electronic traps within the band gap associated to oxygen vacancies. The cathode-luminescence signal, though strongly reduced after an oxidizing treatment, cannot be fully suppressed, indicating the presence of bulk residual oxygen vacancies even in fully oxidized samples. Finally, a third mechanism based on the possibility of La/Sr short-range interdiffusion[18,19] through a few unit cells at the interface, with La^{3+} cations substituting Sr^{2+} in the STO structure, has to be considered.

The first mechanism, based on the polar discontinuity, believed to be at the origin of the q2DEG at the LAO/STO interface, is the most likely. In fact, as shown by Meevasana *et al.*[20] a q2DEG can also be created at the bare $SrTiO_3$ surface, where it is not possible to foresee any cations intermixing, as supported also by a recent study of Reinle-Schmitt *et al.*[21] Moreover defects as a major source for the q2DEG is probably also not very likely due to the large diffusion length of oxygen defects created at the elevated deposition temperatures.

In this paper we show that a giant PPC effect (an increase in conductance at room temperature of about 5 orders of magnitude) that relaxes only well above room temperature can occur in $SrTiO_3/LaAlO_3$ heteroepitaxial structures, activated by an electromagnetic radiation with a wavelength of 395 nm. The characteristic PPC decay time is immeasurably long at room temperature. A decay of PPC with a measurable characteristic time can be achieved only above 500 K.

RESULTS AND DISCUSSION

The LAO films were deposited by pulsed laser deposition with *in situ* reflection high energy electron diffraction (RHEED) diagnostic, onto STO (001) oriented substrates. The LAO film thickness was controlled with a precision of a single unit cell monitoring *in situ* the oscillations of the RHEED specular spot. Figure 1a shows the RHEED intensity oscillations during the film deposition. The good interface quality and the layer-by-layer nature of the growth process is proved by the RHEED diffraction pattern, obtained at the end of the LAO film deposition, which showed typical 2D features (inset of Figure 1a). The LAO film deposition rate and the thickness was estimated, independently from the RHEED intensity oscillations, also by X-ray diffraction size-effect interference fringes. Figure 1b shows the X-ray diffraction size-effect interference fringes obtained for a 22 unit cells thick LAO film deposited onto STO (001) oriented. From the X-ray diffraction size-effect interference fringes calibration and from the RHEED intensity oscillations the thickness of the investigated LAO film was estimated to be about 6.0 nm. Moreover the X-ray diffraction size-effect interference fringes indicate the good crystallographic quality of the deposited LAO films. Finally, to obtain fully oxidized samples, the as-grown STO/LAO interfaces were postannealed in O_2 at 573 K for 12 h in a tubular furnace under visible light. After such an oxidation treatment, the STO/LAO resistance increased, reaching a saturation value larger by a factor of 50 than the value measured for the as-grown samples. This result clearly shows that the conductance of the as-grown samples was mostly due to oxygen deficiency resulting from the deposition process. We argue that the above treatment was able to fill as many as possible of the oxygen vacancies originated by the deposition process and that we obtained fully oxidized samples.

The STO/LAO sheet resistance as a function of the temperature was measured by electrochemical impedance spectroscopy (EIS), for the first time to the best of our knowledge. The EIS technique, compared with the standard DC four probe technique, allows discrimination between purely electronic and ionic or mixed ionic-electronic conduction mechanisms. This circumstance is particularly relevant for the STO/LAO interfaces because stoichiometric STO can be a mixed ionic/electronic conductor,[22] while conduction at the interface is reported to be purely electronic:[9,23] namely,

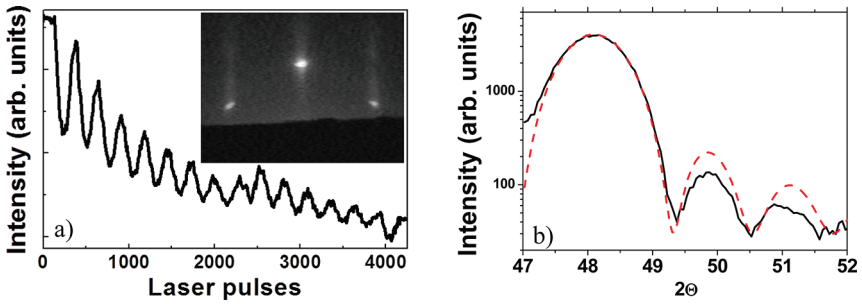

Figure 1. (a) RHEED intensity oscillations obtained during the deposition of a 15 unit cells thick LAO film onto STO (001) oriented substrate. The RHEED diffraction pattern, obtained at the end of the LAO film deposition showed typical 2D features (inset); (b) X-ray diffraction size-effect interference fringes for a LAO film deposited onto STO (001) oriented substrate; the dashed curve (red line) represents a simulation for a 22 unit cells thick LAO film.

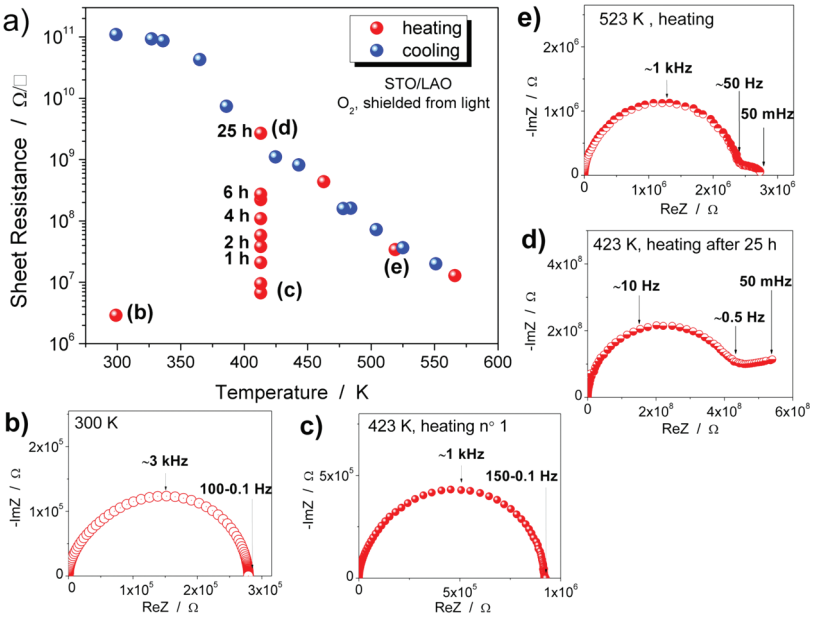

Figure 2. STO/LAO sheet resistance as a function of temperature and time, measured in the dark and O_2 atmosphere, heating (red dots) and cooling (blue dots) the sample between room temperature and 573 K (a). Complex impedance plane plots of the STO/LAO recorded at room temperature (b), after heating the sample at 423 K (c) and maintaining the same temperature for 25 h (d), and further heating at 523 K (e).

using EIS measurements, it is possible to clearly discriminate the electrical response of the STO/LAO interface from the bulk STO substrate contribution. The conductance of the oxygen postannealed STO/LAO and of a STO reference sample was measured by EIS while the samples were kept in a dark environment at an O_2 pressure of 1 atm. Both samples were annealed up to 573 K and successively cooled down to room temperature. A special care was devoted to shielding the samples from any source of light during the thermal treatment. Figure 2 shows the behavior of the STO/LAO sheet resistance ($R_{\square}$) as a function of both temperature and time. At room temperature the sheet resistance remained almost unchanged after one day. At 373 K, a sizable increase in the STO/LAO sheet resistance with time was measured, reaching after 25 h a saturation value about 400 times larger than the initial one at this temperature. Such an effect cannot be explained by a further oxygen uptake. We attribute the large increase in $R_{\square}$ to thermal relaxation of the PPC effect induced by past exposure to light of the STO/LAO heterostructure. Further increasing the temperature up to 573 K resulted in a decrease in $R_{\square}$.

As shown in Figure 2, no hysteretic effects were observed on cooling the sample from 573 to 423 K. On the contrary, $R_{\square}$ below 423 K turned out to be much larger after the thermal treatment in dark environment, with an increase of almost 5 orders of magnitude at room temperature (1×10^{10} Ω/□ instead of 2.5×10^{5} Ω/□). Figure 2 also shows the complex impedance plane plots acquired at room temperature (Figure 2b), as the sample reached the temperature of 423 K (Figure.2c), and at 423 K after 25 h (Figure 2d). At the beginning of the thermal cycle in dark environment, the EIS plots showed only one semicircle without any feature in the low frequency region. Given that Pt

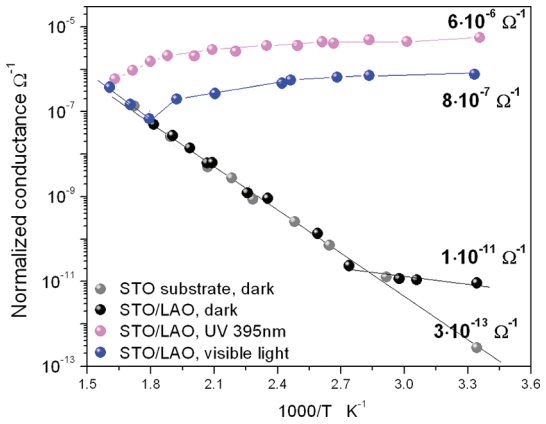

Figure 3. STO/LAO normalized conductance as a function of temperature, after the dark annealing at 573 K, still shielding the sample from any light (black dots), and illuminating the sample by a UV lamp of 395 nm (pink dots) and by visible light (blue dots). Also the STO substrate conductance (gray dots) is reported for comparison.

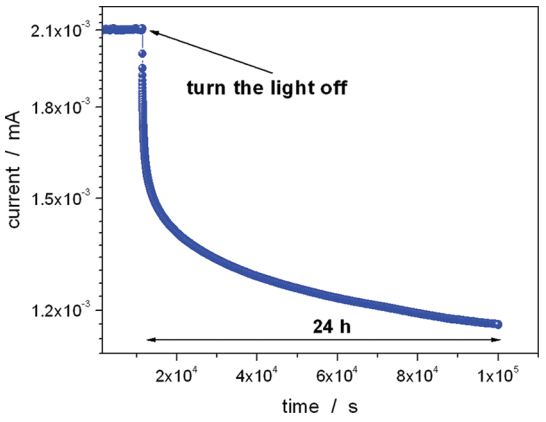

Figure 4. The decay of the induced electronic photoconductivity in a dark environment at room temperature is extremely slow; after 24 h the sample sheet resistance was not even doubled.

electrodes were used, this is clear evidence of pure electronic conductivity. After annealing the sample in dark environment at 423 K for 25 h, not only the value of the sheet resistance (calculated from the intercept of the semicircle with the real axis at low frequency) but also the shape of the EIS plots at low frequency (the electrode response) showed a significant difference, with the appearance of a straight line resulting from electrode polarization. This finding is consistent with the presence of oxygen ions as the main charge carriers in the STO substrate that accumulate at the Pt electrode, which acts as a blocking electrode. At 523 K, the presence of a small semicircle at low frequency, associated to the Pt electrode, indicates a mixed electronic/ionic conduction mechanism, suggesting that the major contribution to conductivity comes from the bulk of the STO rather than from the STO/LAO interface.

Figure 3 summarizes the major results of this paper. We have investigated the photoinduced effects illuminating the STO/LAO sample by both a UV lamp (wavelength 395 nm) and visible light. Figure 3 shows the STO/LAO normalized conductance as a function of the temperature after annealing in dark at 573 K, still shielding the sample from any light (black dots), and illuminating the sample by the UV lamp (pink dots) and by visible light (blue dots). Also the STO substrate conductance (gray dots) is reported for comparison. Figure 3 shows the normalized conductance as a function of temperature in O_2 atmosphere also for a bare STO substrate and the STO/LAO sample after PPC thermal suppression. The black continuous lines are guides for the eye. For the bare STO substrate, a single activation energy of 0.69 eV was observed in the whole temperature range, in agreement with literature data.[24] Similar conductance and activation energy values were measured for the STO/LAO sample above 373 K, indicating that, in this temperature range, the contribution of the interface is negligible. Below 373 K the normalized conductance of STO/LAO diverges from that of the STO substrate, showing a much weaker dependence on temperature. We attribute this contribution to the interfacial q2DEG conductance becoming predominant at low temperatures. Therefore we argue that only below 373 K, the true *intrinsic conductance* of the q2DEG at the interface is observed, while above 373 K the mixed ionic/electronic contribution from the much thicker STO substrate predominates, hindering the intrinsic interface electronic contribution. By intrinsic conductivity we mean the conductivity of a fully oxidized interface where the PPC was suppressed by a suitable thermal treatment in a dark environment. Recently Meevasana *et al.*[20] showed that a q2DEG can be created at the bare $SrTiO_3$ surface and that it is possible to control its carrier density through exposure to ultraviolet radiation. They argued that the irradiation by intense ultraviolet light in ultrahigh vacuum mediates a change in the surface of the $SrTiO_3$, which causes oxygen desorption from the surface and consequently induces the 2DEG.

We performed STO/LAO conductance measurements at room temperature under illumination by UV lamp. To be sure that the oxygen vacancy contribution to the conductivity is negligible, we performed the conductance measurements in an oxygen atmosphere after achieving full oxidation of the samples. Under these experimental conditions, the conductance increased by about 5 orders of magnitude. On the contrary, no PPC effect was detected, as expected,[25] for the bare STO reference sample. A flux of 3×10^{17} photons per second was able to saturate completely the effect in a very short time interval (less than 1 s). Figure 4 shows the decay of the induced electronic photoconductivity in a dark environment at room temperature. The decay is extremely slow; after 24 h the sample sheet resistance was not even doubled, consistently with the results reported by Huijben *et al.*[26]

TABLE 1. Comparison between PPC Values Reported in the Literature for Different Materials

material	ppc effect magnitude	temperature	reference
GaN	3	300 K	25
$Ga_{1-x}In_xN_yAs_{1-y}$	5	150 K	26
$Al_{0.1}Ga_{0.9}N$/GaN	10^2	300 K	27
Si:H multilayer	10^2	300 K	28
Si membranes	10^3	300 K	5
STO/LAO	10^5	300 K	present work

for $(LaO)^+/(TiO_2)^0$ interfaces. This figure must be compared with an increase of 5 orders of magnitude in the sheet resistance that would result from complete suppression of any PPC effect at room temperature. To disentangle the PPC contribution to the conductance mechanism of the q2DEG at the STO/LAO interface, it was necessary to restore the *intrinsic conductance* by thermal annealing, carefully avoiding any lighting of the sample.

While the *intrinsic conductance* of the STO/LAO interface showed a thermally activated behavior, its photoinduced conductance was metallic-like, slightly decreasing as the temperature was increased above room temperature. Above 523 K, the photoinduced conductance started decreasing more rapidly, until collapsing to the bulk STO value at about 623 K.

The reported phenomenon of giant persistent photoconductivity at the STO/LAO interface is quantitatively much larger than any other PPC effect previously reported in the literature. The experimental deposition-annealing protocol followed during the samples preparation and during the photoconductivity measurements plays a fundamental role in the PPC effect values observed in the different studies. Table 1 reports the PPC effect values obtained from the literature for several semiconductors.[5,27−30] It is possible to notice that the PPC effect we discovered at the STO/LAO interface is at least 2 orders of magnitude larger than the largest reported in the literature for rough Si membranes. The giant PPC effect at the STO/LAO interface can be qualitatively explained by the same mechanism active in the case of semiconducting interfaces. The energy associated with the wavelength of our radiation source is just below the band gap of STO (3.2 eV), therefore it is not able to excite hole/electron pairs. However, residual oxygen vacancies behave as electron traps for the electrons. These traps are located inside the energy gap of STO.[31] Once a free electron has been generated by the absorption of a photon, the macroscopic potential barrier due to the positively charged layer at the interface of a TiO_2-terminated STO substrate and the negative electronic space charge region, responsible for the q2DEG, spatially separates the photoexcited electron from the parent donors defect bringing it close to the interface where all traps are already neutralized, thus giving rise to the PPC phenomenon. Although a close connection between giant PPC and q2DEG is not proven the simultaneous occurrence of two striking phenomena such as the q2DEG creation and the giant PPC effects at the LAO/STO interface is probably not fortuitous and deserves a better comprehension.

CONCLUSIONS

Using EIS measurements we have demonstrated, for the first time to the best of our knowledge, that fully oxidized STO/LAO interfaces show a giant PPC effect at room temperature, which can be explained on the same general ground as the PPC effect observed for semiconducting heterostructures. However, different from the effect in standard semiconducting heterostructures, PPC at the STO/LAO interface is persistent even at room temperature and giant as it gives rise to a conductivity increase of about 5 orders of magnitude, the largest ever reported for any semiconducting heterostructures. The room temperature persistence and the giant value of PPC at the STO/LAO interface may renew interest and open new perspectives for the practical exploitation of these heterostructures, such as bistable optical switches[32] and radiation detectors.[33] Moreover, from the viewpoint of understanding fundamental physical mechanisms, it should be noticed that PPC effects must be carefully controlled to unveil the intrinsic behavior of the STO/LAO interfaces, as even a limited exposure to visible light can strongly modify the electrical transport properties of this system even above room temperature, since we clearly demonstrated that only a thermal treatment in a dark environment can completely erase the PPC effect. Furthermore, our conductivity measurements allow concluding that the high conductivity, revealed at the LAO/STO interface at room temperature, is purely electronic.

METHODS

The $LaAlO_3$ films were deposited by pulsed laser deposition, using an excimer laser charged with KrF (248 nm wavelength, pulse width 25 ns, repetition rate 5 Hz). The laser beam, with energy of 200 mJ per pulse, was focused in a vacuum chamber onto a commercial polycrystalline LAO target disk. A substrate of STO (001) oriented single crystal was placed at a distance of about 50 mm from the target on a heated holder. The substrate temperature was maintained constant during the deposition at about 1000 K in an oxygen atmosphere pressure of 5×10^{-2} Pa. After the growth, samples were cooled to room temperature in about 1 h in 1 mbar of molecular oxygen. In these conditions the growth rate was about 1.5×10^{-3} nm per laser shot.

For the electrical measurements, two parallel strip-shaped Ti−Pt electrodes were deposited on the film surface and wired to the read-out electronics using Pt paste and wires. Electron beam deposition was used for the thermal evaporation of Ti and

Pt. Ten nanometers of Ti and 100 nm of Pt films were deposited *in situ* at a base pressure of about 5×10^{-5} Pa to vacuum, using an accelerating voltage of 20 kV and an emission current of about 80 and 250 mA, respectively, achieving a deposition rate of a few Å/s. The electrodes were deposited at room temperature and patterned by a stencil mask. Electrochemical impedance spectroscopy (EIS) measurements were carried out using a multichannel potentiostat VMP3 (Bio-Logic) in the 10 mHz and 1 MHz frequency range.

Conflict of Interest: The authors declare no competing financial interest.

Acknowledgment. This work was partly supported by the World Premier International Research Center Initiative of MEXT, Japan.

REFERENCES AND NOTES

1. Rose, A. *Concepts in Photoconductivity and Allied Problems*; Wiley: New York/London, 1963.
2. Queisser, H. J.; Theodorou, D. E. Hall-Effect Analysis of Persistent Photocurrents in *n*-GaAs Layers. *Phys. Rev. Lett.* **1979**, *43*, 401–404.
3. Li, J. Z.; Lin, J. Y.; Jiang, H. X. Y.; Asif, Khan M.; Chen, Q. Persistent Photoconductivity in a Two-Dimensional Electron Gas System Formed by an AlGaN/GaN Heterostructure. *J. Appl. Phys.* **1997**, *82*, 1227–1230.
4. Calarco, R.; Marso, M.; Richter, T.; Aykanat, A. I.; Meijers, R.; Hart, A.v.d.; Stoica, T.; Lüth, H. Size-Dependent Photoconductivity in MBE-Grown GaN-Nanowires. *Nano Lett.* **2005**, *5*, 981–984.
5. Feng, P.; Monch, I.; Harazim, S.; Huang, G.; Mei, Y.; Schmidt, O. G. Giant Persistent Photoconductivity in Rough Silicon Nanomembranes. *Nano Lett.* **2009**, *9*, 3453–3459.
6. Kudinov, V. I.; Kirilyuk, A.; Kreines, N. M.; Laiho, R.; Läderanta, E. Photoinduced Superconductivity in $YBa_2Cu_3O_{7-x}$ Films. *Phys. Lett. A* **1990**, *151*, 358–364.
7. Shibuya, K.; Ohnishi, T.; Uozumi, T.; Koinuma, H.; Lippmaa, M. An *in Situ* Transport Measurement of Interfaces between $SrTiO_3$(100) Surface and an Amorphous Wide-Gap Insulator. *Appl. Surf. Sci.* **2006**, *252*, 8147–8150.
8. Lang, D. V.; Logan, R. A.; Jaros, M. Trapping Characteristics and a Donor-complex (DX) Model for the Persistent-Photoconductivity Trapping Center in Te-doped $Al_xGa_{1-x}As$. *Phys. Rev. B* **1979**, *19*, 1015–1030.
9. Ohtomo, A.; Hwang, H. Y. A High-Mobility Electron Gas at the $LaAlO_3/SrTiO_3$ Heterointerface. *Nature* **2004**, *427*, 423–426.
10. Thiel, S.; Hammerl, G.; Schmehl, A.; Schneider, C. W.; Mannhart, J. Tunable Quasi-Two-Dimensional Electron Gases in Oxide Heterostructures. *Science* **2006**, *313*, 1942–1945.
11. Nakagawa, N.; Hwang, H. Y.; Muller, D. A. Why Some Interfaces Can Never Be Sharp. *Nat. Mater.* **2006**, *5*, 204–209.
12. Siemons, W.; Koster, G.; Yamamoto, H.; Harrison, W. A.; Lucovsky, G.; Geballe, T. H.; Blank, D. H. A.; Beasley, M. R. Origin of Charge Density at $LaAlO_3$ on $SrTiO_3$ Heterointerfaces: Possibility of Intrinsic Doping. *Phys. Rev. Lett.* **2007**, *98*, 196802.
13. Herranz, G.; Basletic, M.; Bibes, M.; Carretero, C.; Tafra, E.; Jacquet, E.; Bouzehouane, K.; Deranolt, C.; Hamzic, A.; Broto, J.-M.; *et al.* High Mobility in $LaAlO_3/SrTiO_3$ Heterostructures: Origin, Dimensionality, and Perspectives. *Phys. Rev. Lett.* **2007**, *98*, 216803.
14. Scullin, M. L.; Ravichandran, J.; Yu, C.; Huijben, M.; Seidel, J.; Majumdar, A.; Ramesh, R. Pulsed Laser Deposition-Induced Reduction of $SrTiO_3$ Crystals. *Acta Mater.* **2010**, *58*, 457–463.
15. Schneider, C. W.; Esposito, M.; Marozau, I.; Conder, K.; Doebeli, M.; Hu, Yi; Mallepell, M.; Wokaun, A.; Lippert, T. The Origin of Oxygen in Oxide Thin Films: Role of the Substrate. *Appl. Phys. Lett.* **2010**, *97*, 192107.
16. Kan, D.; Terashima, T.; Kanda, R.; Masuno, A.; Tanaka, K.; Chu, S.; Kan, H.; Ishizumi, A.; Kanemitsu, Y.; Shimakawa, Y.; Takano, M. Blue-Light Emission at Room Temperature from Ar^+-Irradiated $SrTiO_3$. *Nat. Mater.* **2005**, *4*, 816–819.
17. Kalabukhov, A.; Gunnarson, R.; Börjesson, J.; Olson, E.; Claeson, T.; Winkler, D. Effects of Oxygen Vacancies in the $SrTiO_3$ Substrate on the Electrical Properties of the $LaAlO_3/SrTiO_3$ Interfaces. *Phys. Rev. B* **2007**, *75*, 121404(R).
18. Willmott, P. R.; Pauli, S. A.; Herger, R.; Schleputz, C. M.; Martoccia, D.; Patterson, B. D.; Delley, B.; Clarke, R.; Kumah, D.; *et al.* Structural Basis for the Conducting Interface between $LaAlO_3$ and $SrTiO_3$. *Phys. Rev. Lett.* **2007**, *99*, 155502.
19. Kalabukhov, A. S.; Boikov, Yu.A.; Serenkov, I. T.; Sakharov, V. I.; Popok, V. N.; Gunnarsson, R.; Borjesson, J.; Ljustina, N.; Olsson, E.; Winkler, D.; *et al.* Cationic Disorder and Phase Segregation in $LaAlO_3/SrTiO_3$ Heterointerfaces Evidenced by Medium-Energy Ion Spectroscopy. *Phys. Rev. Lett.* **2009**, *103*, 146101.
20. Meevasana, W.; King, P. D. C.; He, R. H.; Mo, S. K.; Hashimoto, M.; Tamai, A.; Songsiriritthigul, P.; Baumberger, F.; Shen, Z. X. Creation and Control of a Two-Dimensional Electron Liquid at the Bare $SrTiO_3$ Surface. *Nat. Mater.* **2011**, *10*, 114–118.
21. Reinle-Schmitt, M. L.; Cancellieri, C.; Li, D.; Fontaine, D.; Medarde, M.; Pomjakushina, E.; Schneider, C. W.; Gariglio, S.; Ghosez, Ph.; Triscone, J.-M.; Willmott, P. R.; Intrinsic Origin of the Two-Dimensional Electron Gas at Polar Oxide Interfaces. *arXiv*:1112.3532v1.
22. Rodewald, S.; Fleig, J.; Maier, J. Measurement of Conductivity Profiles in Acceptor-Doped Strontium Titanate. *J. Eur. Ceram. Soc.* **1999**, *19*, 797–801.
23. Reyren, N.; Thiel, S.; Caviglia, A. D.; Kourkoutis, L. F.; Hammerl, G.; Richter, C.; Schneider, C. W.; Kopp, T.; Rüetschi, A. S.; Jaccard, D.; *et al.* Superconducting Interfaces Between Insulating Oxides. *Science* **2007**, *317*, 1196–1199.
24. Guo, X. Comment on "Colossal Ionic Conductivity at Interfaces of Epitaxial ZrO_2:$Y2O_3$/$SrTiO_3$ Heterostructures". *Science* **2009**, *324*, 465a.
25. Kozuka, Y.; Hikita, Y.; Susaki, T.; Hwang, H. Y. Optically Tuned Dimensionality Crossover in Photocarrier-Doped $SrTiO_3$: Onset of Weak Localization. *Phys. Rev. B* **2007**, *76*, 085129.
26. Huijben, M.; Brinkman, A.; Koster, G.; Rijnders, G.; Hilgenkamp, H.; Blank, D. H. A. Structure-Property Relation of $SrTiO_3/LaAlO_3$ Interfaces. *Adv. Mater.* **2009**, *21*, 1665–1667.
27. Chen, H. M.; Chen, Y. F.; Lee, M. C.; Feng, M. S. Persistent Photoconductivity in *n*-Type GaN. *J. Appl. Phys.* **1997**, *82*, 899–901.
28. Li, J. Z.; Lin, J. Y.; Jiang, H. X.; Geisz, J. F.; Kurtz, S. R. Persistent Photoconductivity in $Ga_{1-x}In_xN_yAs_{1-y}$. *Appl. Phys. Lett.* **1999**, *75*, 1899–1901.
29. Hasen, J.; Lederman, D.; Schuller, I. K.; Kudinov, V.; Maenhoudt, M.; Bruynseraede, Y. Enhancement of Persistent Photoconductivity in Insulating High-T, Thin Films. *Phys. Rev. B* **1995**, *51*, 1342–1345.
30. Kakalios, J.; Fritzsche, H. Persistent Photoconductivity in Doping-Modulated Amorphous Semiconductors. *Phys. Rev. Lett.* **1984**, *53*, 1602–1605.
31. Carrasco, J.; Illas, F.; Lopez, N.; Kotomin, E. A.; Zhukovskii, Yu. F.; Evarestov, R. A.; Mastrikov, Yu A.; Piskunov, S.; Maier, J. First-Principles Calculations of the Atomic and Electronic Structure of F Centers in the Bulk and on the (001) Surface of $SrTiO_3$. *Phys. Rev. B* **2006**, *73*, 064106.
32. Tanabe, T.; Notomi, M.; Mitsugi, S.; Shinya, A.; Kuramochi, E. Fast Bistable All-Optical Switch and Memory on a Silicon Photonic Crystal On-Chip. *Opt. Lett.* **2005**, *30*, 2575–2577.
33. Sharma, A. K.; Logofätu, P. C.; Mayberry, C. S.; Brueck, S. R. J.; Islam, N. E. Effects of Dimensional Nanoscaling on the Optical and Electrical Properties of Crystalline Si Thin Films. *J. Appl. Phys.* **2007**, *101*, 104914.